

A Brief Review of the Chan–Vese Paper: *Active Contours Without Edges*

Camilo A. Martínez M., *Universität des Saarlandes*

September 22, 2024

Abstract—This report presents a brief review of the Chan–Vese model proposed in the paper *Active Contours Without Edges* by T. Chan and L. Vese [1], published in 2001. This paper introduced a new model for image segmentation based on the *Mumford–Shah functional* using a powerful mathematical backbone, the level set method [2]. This report provides an overview of the prior works that led to the findings of Chan and Vese, the formulation of the Chan–Vese model, the energy minimization and discretization, its limitations, as well as some qualitative results obtained by the authors. Furthermore, some of the extensions and improvements to the model that came after the publication of the original paper are briefly touched upon. Finally, the report concludes with a discussion of the impact the paper had on future research, specifically in the field of image segmentation.

Index Terms—IEEEtran, paper, journal, *Active Contours Without Edges*, Chan–Vese, image segmentation, Mumford–Shah, level set method.

I. INTRODUCTION

THE paper *Active Contours Without Edges* by Tony Chan and Luminita Vese [1] is a seminal work in the field of image segmentation. It was published in 2001 and introduces a new model for image segmentation based on the *Mumford–Shah functional* [3] using the level set method, proposed by Osher and Sethian [2] in 1988, as the mathematical backbone. The paper has been cited over 8,000 times according to IEEEExplore® and has had a significant impact on the field of *Computer Vision*, particularly in the topic of image segmentation, one of its most widely studied problems. Over the years, it has found an application in medical imaging, robotics, video surveillance, materials science, autonomous driving, and many others.

A. Prior Works

Before the Chan–Vese model, some early methods existed for image segmentation, namely, thresholding, region growing, and edge-based segmentation. Some improvements were made with the introduction of the *snakes* and *active contours* models by Kass et al. [4]. Nevertheless, the challenge of segmenting images without clear edges remained. Table I shows a list of some of the prior founding works that led to the development of the Chan–Vese model.

This document template was developed by the IEEE Publication Technology Department, distributed under the L^AT_EX Project Public License (LPPL) (<http://www.latex-project.org/>) version 1.3. A copy of the LPPL, version 1.3, is included in the base L^AT_EX documentation of all distributions of L^AT_EX released 2003/12/01 or later. The opinions expressed here are entirely that of the author. No warranty is expressed or implied.

TABLE I: Prior Works to the Chan–Vese Model

Title	Authors	Year
Boundary detection by minimizing functionals [3]	D. Mumford and J. Shah	1985
Snakes: Active contour models [4]	M. Kass et al.	1988
A topology independent shape modeling scheme [5]	R. Malladi et al.	1993
On geodesic active contours [6]	V. Caselles et al.	1997

II. THE CHAN–VESE MODEL

A. The “Fitting” Problem

T. Chan and L. Vese (2001) proposed a specific region-based active contour model, where the image is segmented into **two phases/regions**: object and background. A summary of the mathematical derivation of the model is presented below.

Assume we have an image $u(\mathbf{x})$, $\mathbf{x} \in \Omega$, and the image is formed by two regions with mean intensity values: u_{in} and u_{out} . Our *evolving* boundary curve C separates the two regions. Then, we can define a *fitting* term that penalizes deviations from the mean intensity values:

$$\text{fitting}(C) := F_{in}(C) + F_{out}(C) \quad (1)$$

Furthermore, using a Mean-Squared Error (MSE) approach, equation (1) can be developed as:

$$\begin{aligned} \text{fitting}(C) &= F_{in}(C) + F_{out}(C) \\ &= \underbrace{\int_{in(C)} |u(\mathbf{x}) - c_{in}|^2 d\mathbf{x}}_{> 0, \text{ if } u(\mathbf{x}) \text{ deviates from } c_{in}} + \underbrace{\int_{out(C)} |u(\mathbf{x}) - c_{out}|^2 d\mathbf{x}}_{> 0, \text{ if } u(\mathbf{x}) \text{ deviates from } c_{out}} \end{aligned}$$

Thus, the minimizer C_0 that satisfies $\text{fitting}(C_0) \approx 0$, which is the contour that segments the image into the two regions with mean intensity values c_{in} and c_{out} , can be defined as:

$$C_0 = \inf_C \{\text{fitting}(C)\} = \inf_C \{F_{in}(C) + F_{out}(C)\} \quad (2)$$

Figure 1 shows the different cases of the fitting term for different contours C that enclose the object in the image. The objective C_0 is the one that perfectly encloses the object, i.e., $\text{fitting}(C_0) = 0$, as shown in the lower-right example.

B. Formulation as an Energy Functional

Now, we can introduce the energy functional $F(C)$ as:

$$F(C) = \underbrace{\mu \cdot \text{Length}(C) + \nu \cdot \text{Area}(in(C))}_{\text{penalize the "size" of } C} + \text{fitting}(C) \quad (3)$$

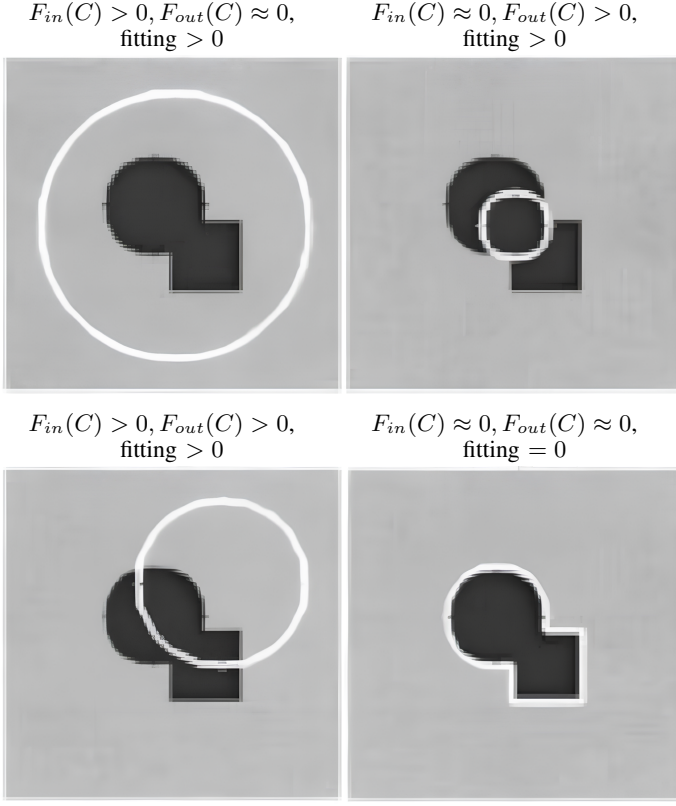


Fig. 1: Consider all possible cases of C enclosing the object in the image. The *fitting* term is minimized only in the case when C is exactly on the boundary of the object [1].

Thus, the energy minimization problem becomes:

$$C_0 = \inf_C F(C) \quad (4)$$

with

$$\begin{aligned} F(C) = & \mu \cdot \text{Length}(C) + \nu \cdot \text{Area}(\text{in}(C)) \\ & + \lambda_1 \int_{\text{in}(C)} |u(\mathbf{x}) - c_{in}|^2 d\mathbf{x} \\ & + \lambda_2 \int_{\text{out}(C)} |u(\mathbf{x}) - c_{out}|^2 d\mathbf{x} \end{aligned} \quad (5)$$

where $\mu, \nu \in \mathbb{R}_0^+, \lambda_1, \lambda_2 \in \mathbb{R}^+$ are fixed parameters. This can be formulated and solved using the **level set method** [2], as presented in Sec. II-D.

C. Comparison with the Mumford–Shah Model

The *Mumford–Shah model* introduced in 1985 [3] by D. Mumford and J. Shah is defined as [7]:

$$E_{MS}(K, u) = \int_{\Omega} (f - u)^2 dx + \gamma \int_{\Omega \setminus K} |\nabla u|^2 dx + \lambda |K|$$

This model leads to the **Chan–Vese approach**

- if we have piecewise constant approximations u , i.e., $u = \text{constant } c_i$ on each connected component R_i of $\Omega \setminus C$.
- and an edge set K that separates Ω into two phases.

This reduced case is called the *minimal partition problem* [1].

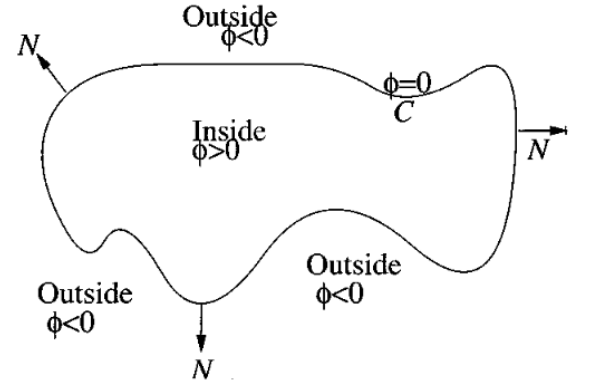


Fig. 2: Illustration of the relationship between C and ϕ ; Curve $C = \{(x, y) : \phi(x, y) = 0\}$ propagating in normal direction [1].

D. The Level-Set Formulation

In the level set method [2], $C \subset \Omega$ is represented by the zero level set of a *Lipschitz function* $\phi : \Omega \rightarrow \mathbb{R}$, such that

$$\begin{aligned} C &= \partial\omega = \{(x, y) \in \Omega : \phi(x, y) = 0\}, \\ \text{in}(C) &= \omega = \{(x, y) \in \Omega : \phi(x, y) > 0\}, \\ \text{out}(C) &= \Omega \setminus \bar{\omega} = \{(x, y) \in \Omega : \phi(x, y) < 0\}. \end{aligned}$$

Intuitively, this *Lipschitz function* ϕ is by definition limited in how fast it can change: there exists a real number such that, for every pair of points on the graph of this function, the absolute value of the slope of the line connecting them is not greater than a real number called the *Lipschitz constant* of the function, L [8]. See figure 2 for an illustration of how C and ϕ are related to each other.

Now, our aim is to compute the *Euler-Lagrange* equation associated with the introduced energy functional $F(C)$ of equation (3) by replacing the unknown variable C by the new variable ϕ [9].

On the other hand, we can define the *Heaviside* function $H(z)$ and the *Dirac delta* function $\delta_0(z)$ as:

$$H(z) = \begin{cases} 0, & \text{if } z < 0 \\ 1, & \text{if } z \geq 0 \end{cases}, \quad \delta_0(z) = \frac{d}{dz} H(z) = \begin{cases} \infty, & \text{if } z = 0, \\ 0, & \text{if } z \neq 0 \end{cases}$$

These functions, when applied to ϕ , allow us to compute the *length* and *area* of the curve C , as defined below and illustrated in figure 3:

$$\text{Length}\{\phi = 0\} = \int_{\Omega} |\nabla H(\phi(\mathbf{x}))| d\mathbf{x} = \int_{\Omega} \delta_0(\phi(\mathbf{x})) |\nabla \phi(\mathbf{x})| d\mathbf{x} \quad (6)$$

$$\text{Area}\{\phi \geq 0\} = \int_{\Omega} H(\phi(\mathbf{x})) d\mathbf{x} \quad (7)$$

Thus, using equations 6 and (7) in (5), we can rewrite the

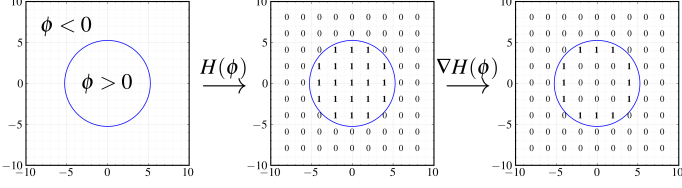


Fig. 3: From **left** to **right**, the process of applying H to ϕ and then taking the gradient.

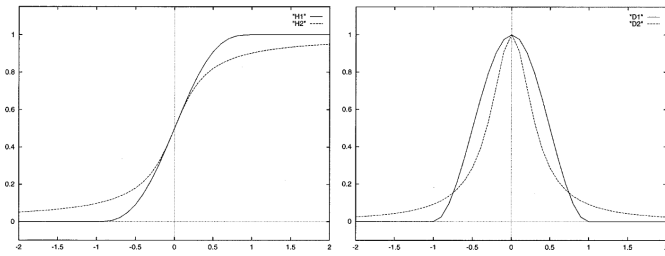


Fig. 4: Two different regularizations of the (left) heaviside function H and (right) delta function δ_0 [1].

energy functional $F(C)$ as:

$$\begin{aligned} F(\phi) = & \underbrace{\mu \int_{\Omega} \delta(\phi(\mathbf{x})) |\nabla \phi(\mathbf{x})| d\mathbf{x}}_{\text{Length}(C)} + \nu \underbrace{\int_{\Omega} H(\phi(\mathbf{x})) d\mathbf{x}}_{\text{Area}(in(C))} \\ & + \lambda_1 \underbrace{\int_{\Omega} |u(\mathbf{x}) - c_{in}|^2 H(\phi(\mathbf{x})) d\mathbf{x}}_{= \int_{in(C)} |u(\mathbf{x}) - c_{in}|^2 d\mathbf{x}} \\ & + \lambda_2 \underbrace{\int_{\Omega} |u(\mathbf{x}) - c_{out}|^2 (1 - H(\phi(\mathbf{x}))) d\mathbf{x}}_{= \int_{out(C)} |u(\mathbf{x}) - c_{out}|^2 d\mathbf{x}} \end{aligned}$$

In practice, H and δ_0 are approximated by *continuous functions* H_ϵ and δ_ϵ , respectively, such that H_ϵ is at least $C^2(\bar{\Omega})$ and $\lim_{\epsilon \rightarrow 0} H_\epsilon(z) = H(z)$ and $\lim_{\epsilon \rightarrow 0} \delta_\epsilon(z) = \delta_0(z)$. The regularized functions analyzed by the authors are shown in figure 4 and further explained in Sec. III-A.

Finally, our *regularized* energy functional $F_\epsilon(\phi)$ is given by:

$$\begin{aligned} F(\phi) = & \mu \int_{\Omega} \delta_\epsilon(\phi(\mathbf{x})) |\nabla \phi(\mathbf{x})| d\mathbf{x} + \nu \int_{\Omega} H_\epsilon(\phi(\mathbf{x})) d\mathbf{x} \\ & + \lambda_1 \int_{\Omega} |u(\mathbf{x}) - c_{in}|^2 H_\epsilon(\phi(\mathbf{x})) d\mathbf{x} \\ & + \lambda_2 \int_{\Omega} |u(\mathbf{x}) - c_{out}|^2 (1 - H_\epsilon(\phi(\mathbf{x}))) d\mathbf{x} \end{aligned}$$

E. Energy Minimization & Discretization

The *Euler–Lagrange equation* for an energy functional of the form is given by the following expression:

$$E(\phi) = \int_{\Omega} F(x, y, \phi, \phi_x, \phi_y) d\mathbf{x} \implies F_\phi - \partial_x F_{\phi_x} - \partial_y F_{\phi_y} = 0$$

with *natural boundary conditions*

$$\mathbf{n}^\top \begin{pmatrix} F_{\phi_x} \\ F_{\phi_y} \end{pmatrix} = 0$$

where \mathbf{n} denotes a normal vector to the image boundary $\partial\Omega$.

In our case study, remembering that we are keeping c_{in} and c_{out} fixed, and minimizing F_ϵ with respect to ϕ , we deduce the associated *Euler–Lagrange* equation for ϕ :

$$\begin{cases} F_\phi &= \nu \delta_\epsilon(\phi) + \lambda_1 |u - c_{in}|^2 \delta_\epsilon(\phi) - \lambda_2 |u - c_{out}|^2 \delta_\epsilon(\phi), \\ F_{\phi_x} &= 2\mu \delta_\epsilon(\phi) \phi_x, \\ F_{\phi_y} &= 2\mu \delta_\epsilon(\phi) \phi_y \end{cases}$$

Thus, for $t \geq 0$, we get:

$$\begin{aligned} \frac{\partial \phi}{\partial t} &= \delta_\epsilon(\phi) \left[\mu \operatorname{div} \left(\frac{\nabla \phi}{|\nabla \phi|} \right) - \nu - \lambda_1 (u - c_{in})^2 + \lambda_2 (u - c_{out})^2 \right] \\ &= 0 \quad \text{in } (0, \infty) \times \Omega \end{aligned} \tag{8}$$

With initial contour $\phi(0, x, y) = \phi_0(x, y)$ in Ω and boundary condition:

$$\frac{\delta_\epsilon(\phi)}{|\nabla \phi|} \frac{\partial \phi}{\partial \vec{n}} = 0 \quad \text{on } \partial\Omega \tag{9}$$

where \vec{n} denotes the exterior normal to the boundary $\partial\Omega$, and $\partial\phi/\partial\vec{n}$ denotes the normal derivative of ϕ at the boundary.

To discretize and linearize the PDE given by (8) in ϕ , Chan and Vese (2001) used a *finite differences implicit scheme*.

$$\begin{aligned} \frac{\phi_{i,j}^{n+1} - \phi_{i,j}^n}{\Delta t} &= \delta_h(\phi_{i,j}^n) \left[\frac{\mu}{h^2} \Delta_-^x \right. \\ &\quad \cdot \left(\frac{\Delta_+^x \phi_{i,j}^{n+1}}{\sqrt{(\Delta_+^x \phi_{i,j}^n)^2/(h^2) + (\phi_{i,j+1}^n - \phi_{i,j-1}^n)^2/(2h)^2}} \right) \\ &\quad + \frac{\mu}{h^2} \Delta_-^y \cdot \left(\frac{\Delta_+^y \phi_{i,j}^{n+1}}{\sqrt{\frac{(\phi_{i+1,j}^n - \phi_{i-1,j}^n)^2}{(2h)^2} + \frac{(\Delta_+^y \phi_{i,j}^n)^2}{h^2}}} \right) \\ &\quad \left. - \nu - \lambda_1 (u_{i,j} - c_1(\phi^n))^2 + \lambda_2 (u_{i,j} - c_2(\phi^n))^2 \right] \end{aligned}$$

III. RESULTS

A. Parameter Selection

- $\lambda_1 = \lambda_2 = 1$, $\nu = 0$, $h = 1$ (the step space), $\Delta t = 0.1$ (the time step).
- $H_{2,\epsilon}$ and $\delta_{2,\epsilon}$ were used with $(\epsilon = h = 1)$, in order to automatically detect *interior contours*, and to ensure the computation of a *global minimizer*. This is illustrated in figure 4, where $H_{2,\epsilon}$ and $\delta_{2,\epsilon}$ are shown to never reach zero, whereas $H_{1,\epsilon}$ and $\delta_{1,\epsilon}$ do. This means that the latter will not take into account global contributions, but only local ones, and thus will lead to a local minimizer of the energy [1].
- μ is *experiment-dependent*, i.e. if our goal is to
 - detect as many objects as possible \implies small μ .
 - detect only larger objects \implies large μ .

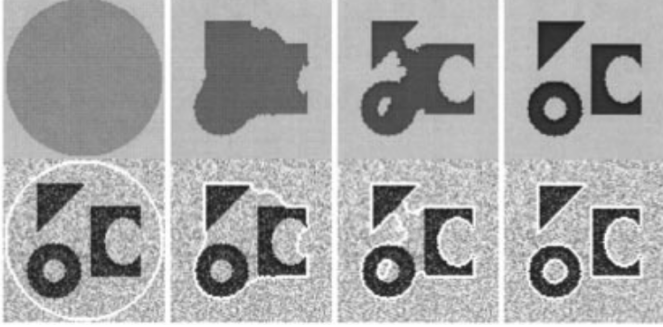


Fig. 5: Detection of different objects from a noisy image, with various shapes and with an interior contour. **Bottom:** u and the contour. **Top:** the piecewise-constant approximation of u . Size = 100×100 , $\phi_0(x, y) = -\sqrt{(x - 50.5)^2 + (y - 50.5)^2} + 48.5$, $\mu = 0.1 \times 255^2$, no reinitialization, cpu = 4.60 s [1].

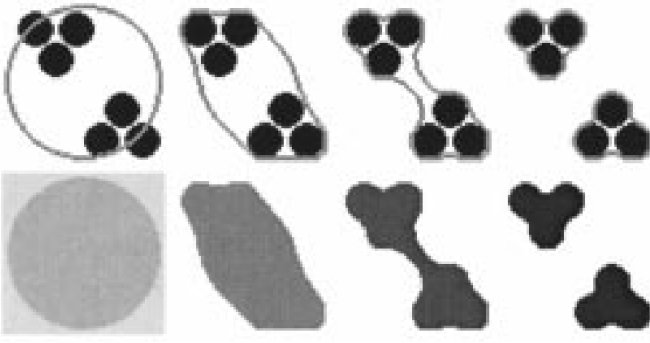


Fig. 6: Grouping based on Kanizsa's "proximity rule." Size = 64×64 , $\phi_0(x, y) = -\sqrt{(x - 32.5)^2 + (y - 32.5)^2} + 30$, $\mu = 2 \cdot 255^2$, no reinitialization, cpu = 5.76 s [1].

B. Qualitative results

Figure 5 shows that the model works on a noisy synthetic image, with various shapes and an interior contour, which is automatically detected, without considering a second initial curve. Due to the level set implementation, the model allows an automatical change of topology, which is not affected by blurred boundaries or even lines not necessarily closed [1].

On the other hand, figure 6 shows an application of the model in detecting objects defined by a grouping according to Kanizsa's "proximity rule". This grouping can also be based on the chromatic resemblance or identity, among objects of the same shape or orientation [1]. Refer to the Sec. IV-A for more qualitative results.

C. Limitations of the Model

- The Chan–Vese model is a specific case of the *Mumford–Shah functional*, meaning it is limited to piecewise constant approximations of the image. Thus, it is not a general solution to the segmentation problem.
- There are objects which cannot be detected using the *average intensity value* only, as illustrated in figure 7.

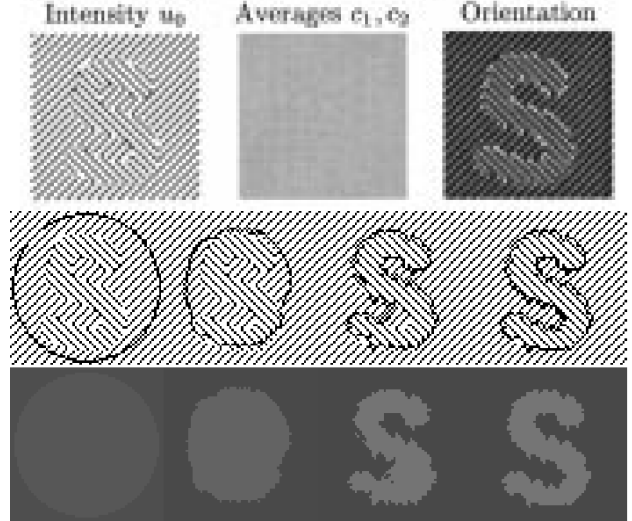


Fig. 7: Grouping based on orientation identity. The original image u (**top**) is replaced by the orientation of the normal to the level curves of u . Size: 64×64 , $\mu = 0.025 \cdot 255^2$, $\nu = 0.02 \cdot 255^2$, $\phi_0(x, y) = -\sqrt{(x - 32.5)^2 + (y - 32.5)^2} + 30$, five iterations of reinitialization, cpu = 10.25 s [1].

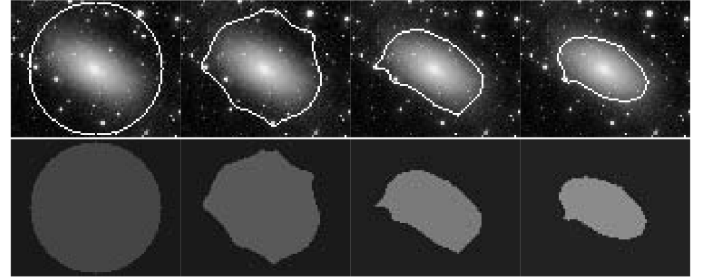


Fig. 8: Detection of a galaxy with very smooth boundaries [1].

IV. IMPACT ON RESEARCH

A. Real-World Applications

Some of the real-world applications of the Chan–Vese model include: detection of minefields using reconnaissance aircraft images that identify many objects that are not mines; detection of Europe night-lights; detection of blurred contours of a galaxy, as shown in figure 8; and detection of a tumor in a MRI image, as shown in figure 9 [1]. It is important to point out that these results are not possible using classical snakes or active contours based on the gradient.

B. Extensions of the Chan–Vese Model

Some modifications of the Chan–Vese model include [7]:

- More sophisticated features than the grey value, such as colour channels, texture features, optic flow fields, etc.
- Additional statistical characterizations of a region, that is, not only mean, but also standard deviation, skewness, kurtosis, etc.
- A-priori knowledge, using a statistical characterization of the shapes to be expected.

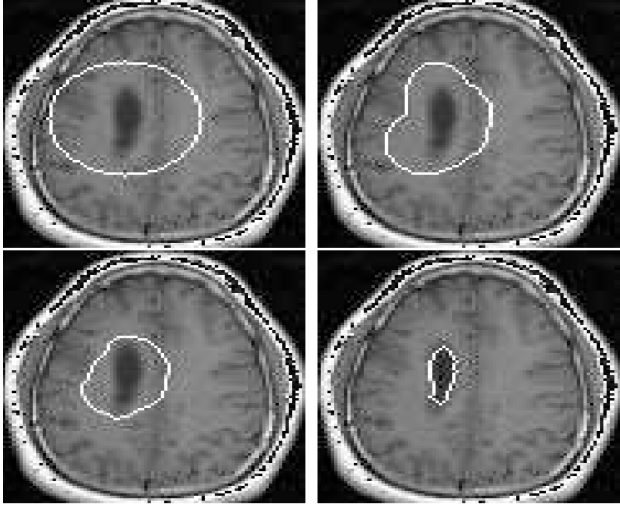


Fig. 9: Detection of a tumor in a MRI image [1].

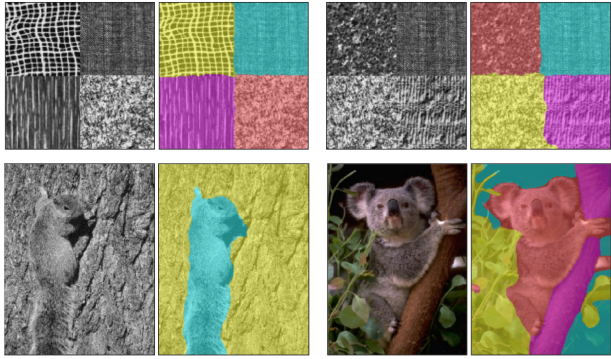


Fig. 10: **Top:** Segmentation of two artificial texture images. **Bottom** Segmentation of color images [10].

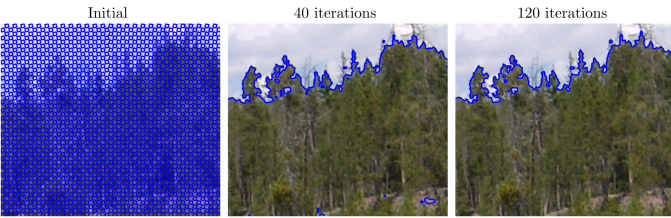


Fig. 11: The Chan–Sandberg–Vese (2000) [11] method can be used to segment color images [12].

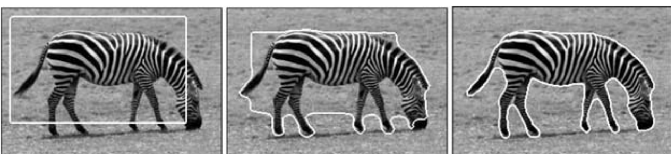


Fig. 12: Curve evolution for the segmentation of a zebra image. Here, a rectangle is used as initialization but small circles also lead to a similar result [13].

All of these extensions have already been studied in the literature over the years. Some of the key papers are listed [here](#), courtesy of [@ConnectedPapers](#).

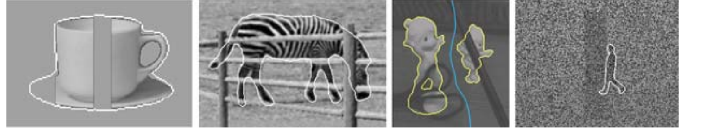


Fig. 13: Sample segmentations using statistical shape priors. From left to right, the shape priors are a single static shape prior, uniformly distributed in the PCA subspace, automatically selected from multiple shape instances [13].

V. CONCLUSION

T. Chan and L. Vese (2001) introduced an active contour model, that does not rely on gradient computation, based on the *Mumford–Shah functional* [3] and the level set method [2], is robust to noise, does and is capable of detecting objects with non-gradient and smooth boundaries. Furthermore, it efficiently identifies interior contours with a single flexible initial curve, which does not need to encircle the target objects.

In conclusion, the Chan–Vese model represented a significant breakthrough in image segmentation, which laid the groundwork for more advanced image segmentation techniques, despite its limitations briefly touched in Sec. III-C. Its legacy is evident in its widespread adoption and the continuous exploration of its potential for addressing complex image analysis challenges.

REFERENCES

- [1] T. Chan and L. Vese, “Active contours without edges,” *IEEE Transactions on Image Processing*, vol. 10, no. 2, pp. 266–277, 2001.
- [2] S. Osher and J. A. Sethian, “Fronts propagating with curvature-dependent speed: Algorithms based on hamilton-jacobi formulations,” *Journal of Computational Physics*, vol. 79, no. 1, pp. 12–49, 1988.
- [3] D. Mumford and J. Shah, “Boundary detection by minimizing functionals,” *IEEE CVPR*, vol. 17, pp. 22–26, 01 1985.
- [4] M. Kass, A. Witkin, and D. Terzopoulos, “Snakes: Active contour models,” *International Journal of Computer Vision*, vol. 1, pp. 321–331, 1988.
- [5] R. Malladi, J. A. Sethian, and B. C. Vemuri, “A topology independent shape modeling scheme,” in *Proc. SPIE Conf. Geometric Methods Computer Vision II*, vol. 2031, San Diego, CA, 1993, pp. 246–258.
- [6] V. Caselles, R. Kimmel, and G. Sapiro, “On geodesic active contours,” *International Journal of Computer Vision*, vol. 22, pp. 61–79, 1997.
- [7] P. Pascal, “Differential equations in computer vision, lecture 25: Self-snakes and active contours,” 2023, universität des Saarlandes.
- [8] W. contributors. (2024) Lipschitz continuity — Wikipedia, the free encyclopedia. Retrieved from https://en.wikipedia.org/wiki/Lipschitz_continuity ([Online; accessed 23.06.2024]).
- [9] H.-K. Zhao, T. Chan, B. Merriman, and S. Osher, “A variational level set approach to multiphase motion,” *Journal of Computational Physics*, vol. 127, pp. 179–195, 1996.
- [10] T. Brox and J. Weickert, “Level set based image segmentation with multiple regions,” in *Pattern Recognition*, C. E. Rasmussen, H. H. Bülthoff, B. Schölkopf, and M. A. Giese, Eds. Berlin, Heidelberg: Springer Berlin Heidelberg, 2004, pp. 415–423.
- [11] T. F. Chan, B. Sandberg, and L. A. Vese, “Active contours without edges for vector-valued images,” *Journal of Visual Communication and Image Representation*, vol. 11, pp. 130–141, 2000, available: <http://dx.doi.org/10.1006/jvc.1999.0442>.
- [12] P. Getreuer, “Chan-vese segmentation,” *Image Processing On Line*, vol. 2, pp. 214–224, 2012, available: <https://doi.org/10.5201/ipol.2012.g-cv>.
- [13] D. Cremers, “Dynamical statistical shape priors for level set-based tracking,” *IEEE Transactions on Pattern Analysis and Machine Intelligence*, vol. 28, no. 8, pp. 1262–1273, 2006.